

Chirp Parameter Optimization and Distributed Detection for Cooperative RSMA-AFDM Systems

Qingyu Li, Guanghui Liu, *Senior Member, IEEE*, Yusha Liu, Fuchen Xu, Chengxiang Liu, Hongjun Liu, and Liaoyuan Zeng

Abstract—Affine frequency division multiplexing (AFDM) exhibits excellent Doppler robustness and the ability to characterize doubly selective channels. However, its signal dispersion characteristics make it challenging to directly adopt traditional time-frequency multiple access schemes. To address this issue, we introduce the cooperative rate splitting multiple access (RSMA) for AFDM systems. The flexible configuration of AFDM chirp parameters can reduce the correlation between users' equivalent channels, which decreases the interference from RSMA private streams. We conduct a theoretical analysis of the cooperative RSMA-AFDM system and demonstrate that minimizing the overlap in the channel column spaces among users can effectively enhance the system performance. Guided by this analysis, we design a chirp parameter optimization scheme that reduces multi-user interference and maximizes diversity gain. To fully exploit the diversity gain brought by the proposed chirp parameter optimization, two expectation propagation (EP)-based distributed cooperative detection schemes are proposed. First, a decision fusion-based method is developed, where local information and cooperative information are fused by maximum ratio combining, achieving a globally consistent estimate of the common stream. Second, we develop a belief-consensus EP-based detection scheme. In each iteration, user nodes exchange and fuse the first- and second-order statistics of the common stream, and the resulting beliefs gradually converge to a consistent global decision, which significantly improves the overall reliability.

Index Terms—Affine frequency division multiplexing (AFDM), rate splitting multiple access (RSMA), distributed cooperative detection, belief consensus, expectation propagation (EP), chirp parameter optimization, doubly selective channels.

I. INTRODUCTION

NEXT-generation mobile communication systems must support a wider range of services and massive user access, which poses significant challenges, especially in high-mobility scenarios such as non-terrestrial networks (NTN) and intelligent transportation systems [1]. High-speed movement of terminals causes large Doppler shifts, disrupting the inherent orthogonality of the widely adopted multicarrier scheme, orthogonal frequency division multiplexing (OFDM) [2], and demands substantial pilot overhead for channel estimation. Another multicarrier modulation, orthogonal time frequency

space (OTFS) [3], which has received widespread attention in recent years, can characterize high Doppler channels in a sparse and stable manner in the delay-Doppler (DD) domain [4], [5]. However, Doppler shifts in practical channels are generally not integer multiples of the sampling interval. These fractional Doppler shifts cause energy leakage, which introduces the non-sparse equivalent channel in the DD domain and can lead to considerable channel-estimation overhead [6]–[8].

Recently, in order to effectively mitigate Doppler spread, affine frequency division multiplexing (AFDM) [9] is developed to modulate and multiplex signals in the discrete affine Fourier transform (DAFT) domain. Unlike OFDM, in which each subcarrier has a fixed frequency, AFDM uses chirp subcarriers whose instantaneous frequencies vary linearly with time [10]. Because the frequency of a chirp also changes linearly under Doppler effect, the received signal remains a chirp when Doppler shifts occur. Mathematically, the set of chirp basis functions is approximately closed under Doppler shifts, which makes AFDM inherently robust to Doppler effects [9], [11], [12]. In addition, AFDM can achieve full channel diversity with one-dimensional signals, thereby significantly reducing transmission latency compared with block-based modulation such as OTFS [13], [14]. Even in the presence of fractional Doppler shifts, the equivalent channel matrix of an AFDM system remains highly sparse [15]. Therefore, in high-mobility scenarios, the channel-estimation overhead of AFDM is substantially lower than that of OFDM and OTFS.

However, for transform-domain multicarrier modulation schemes such as AFDM and OTFS, traditional orthogonal multiple access (OMA) methods in the time-frequency (TF) domain cannot be directly applied. In these systems, each transmitted symbol is spread over the entire TF domain, so symbols from different users completely overlap in TF resources. As a result, simple orthogonal partitioning along the time or frequency dimension alone cannot provide effective user separation and resource allocation. A scheme based on the point-constrained inverse symplectic finite Fourier transform (ISFFT) is proposed in [16] to confine each user's symbols to a limited region in the TF domain and thus enable user separation. Nevertheless, this constraint substantially reduces the inherent channel diversity gain of transform-domain modulation. Designing a multiple-access mechanism that preserves the diversity advantages of transform-domain waveforms while supporting efficient user separation therefore remains a key challenge for future high-mobility, large-scale connectivity systems.

In transform-domain modulation schemes, the adoption of non-orthogonal multiple access (NOMA) technology provides

This work was supported by the Hainan Province Science and Technology Plan Projects under Grant ZDYF2025(LALH)001 and Grant ZDYF2025(LALH)003, and Natural Science Foundation of China (Grant No. 62301123). (*Corresponding author: Guanghui Liu*).

Qingyu Li, Guanghui Liu, Yusha Liu, Fuchen Xu, Chengxiang Liu, Hongjun Liu, Liaoyuan Zeng are with the School of Information and Communication Engineering, University of Electronic Science and Technology of China, Chengdu 611731, China (e-mail: qingyu.li@std.uestc.edu.cn; guanghuiliu@uestc.edu.cn; yusha.liu@uestc.edu.cn; fuchenxu@std.uestc.edu.cn; cxliu@std.uestc.edu.cn; hljliu@std.uestc.edu.cn; lyzeng@uestc.edu.cn).

a feasible method to address multi-user challenges, primarily including power-domain NOMA and code-domain NOMA. The combination of OTFS and sparse code multiple access (SCMA) has been proposed in [17], demonstrating that the block modulation structure of OTFS can bring higher asymptotic diversity gain to the OTFS-SCMA system. However, in this scheme, detection errors in OTFS propagate into the SCMA decoder, leading to performance degradation. To mitigate the error propagation, a cross-domain iterative OTFS detection and SCMA decoding scheme has been proposed in [18] and deep learning (DL)-based scheme [19] is studied. Additionally, iterative detection and SCMA decoding have been implemented and verified in AFDM systems [20]. Another effective approach is power-domain NOMA, which superimposes the signals of different users on the same time–frequency resources [21]. The integration of power-domain NOMA with OTFS demonstrates superior performance in terms of error rate and system capacity compared to traditional NOMA-OFDM systems [22]. An NOMA-OTFS detection scheme based on improved least squares with QR factorization (mLSQR) is proposed in [23]. Furthermore, in [24], an alternating optimization method (AO-MRA) is proposed for multidimensional resource allocation in NOMA-OTFS.

However, directly extending power-domain NOMA, which is designed for single-antenna systems, to multiple input multiple output (MIMO) systems fails to fully exploit the gain brought by multi-antenna configurations, resulting in a reduction of spatial multiplexing gain and spatial degrees of freedom [25], [26]. Power-domain NOMA primarily enhances spectral efficiency through power allocation and successive interference cancellation (SIC), yet its potential for spatial multiplexing and interference management remains relatively limited [27]. It is noteworthy that both SCMA and NOMA are designed to superimpose multi-user signals for transmission over the same resources, thereby improving spectral efficiency. This design principle fundamentally differs from that of multi-antenna systems, aiming to separate data streams and suppress interference in the spatial dimension [28], [29].

Rate splitting multiple access (RSMA) [30], [31] is a promising and novel strategy for non-orthogonal transmission, which has attracted widespread attention in recent years [32]–[35]. In a downlink RSMA system, the transmitted signal for each user is split into a common part and a private part, with all users' common parts combined into a common stream for transmission. At the receiver, each user first decodes and eliminates the common stream before retrieving its own private stream. In this way, RSMA not only achieves efficient interference management, but also fully utilizes the spatial multiplexing gain of multi-antenna systems. Compared with power-domain NOMA, which passively handles strong interference through SIC, RSMA actively controls interference at the transmitter by leveraging spatial degrees of freedom [25]. It converts the inter-user partial interference into decodable common information, thereby more efficiently obtaining the gain provided by multi-antenna systems [29]. In contrast to space division multiple access (SDMA), RSMA significantly enhances system interference resistance and transmission robustness by partially decoding interference [27]. Hence, RSMA

demonstrates high spectral efficiency and strong interference coordination potential in multi-user MIMO systems.

Cooperative communication and RSMA achieve a synergistic integration [36]. In cooperative transmission scenarios, after decoding their own private stream and the common stream, user terminals can further forward the common stream to cell-edge users, thereby significantly enhancing the decoding reliability of the common stream for edge users. Leveraging this mechanism, RSMA can effectively address wide-ranging variations in propagation conditions caused by differences in user channel strengths and directions. This can compensate for performance degradation due to severe path loss, and ultimately extend the system coverage [27], [36]. Cooperative integrated sensing and communication (ISAC)-RSMA systems have been explored in [37]–[39]. By jointly optimizing precoding and rate allocation, a cooperative RSMA scheme is proposed in [40] to address fairness issues in dense visible light communication systems.

In this paper, we investigate the potential of integrating cooperative RSMA with AFDM. We theoretically analyze the diversity gain of the proposed cooperative RSMA-AFDM system. Based on the analytical results, the correlation between equivalent channels is reduced by leveraging the flexible AFDM chirp parameter configuration. This reduction in correlation further enhances the cooperative diversity gain of the cooperative RSMA-AFDM system. To fully obtain this gain, we propose two distributed cooperative expectation propagation (EP)-based detection schemes, including a decision fusion-based scheme and a belief consensus-based scheme.

The main contributions of this paper are summarized below:

- We propose a cooperative RSMA-AFDM system. Cooperative RSMA effectively addresses the multiple access problem in AFDM while fully exploiting the multiplexing gain provided by the spatial degrees of freedom in multi-antenna systems to enhance spectral efficiency. Furthermore, the inherent flexibility of AFDM chirp parameter offers additional performance gain for cooperative RSMA systems, including reduced multi-user interference and enhanced diversity.
- We investigate the diversity gain of the cooperative RSMA-AFDM system by means of pairwise error probability (PEP) analysis. The results prove that the diversity gain of the cooperative RSMA-AFDM system is maximized when the path overlap between different users' DAFT domain equivalent channels is minimized.
- Based on the PEP analysis, we formulate an optimization problem aimed at maximizing the diversity gain of the cooperative RSMA-AFDM system. To solve this problem, we then propose an optimization method based on differentiated AFDM chirp parameters and derive the optimal chirp parameters for different user nodes. The results show that the proposed scheme effectively suppresses multi-user interference and significantly enhances the cooperative diversity gain.
- To fully exploit the cooperative diversity gain brought by chirp parameter optimization, we propose two distributed cooperative algorithms for common stream detection. The first decision fusion-based method combines the

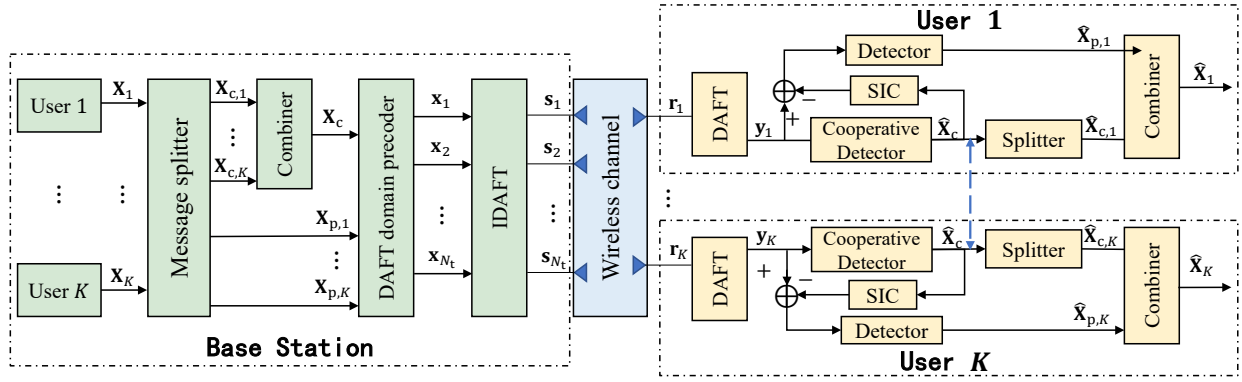


Fig. 1. Block diagram of the downlink cooperative RSMA-AFDM system.

information from local EP detection with information broadcast by other users via MRC to achieve a globally consistent distributed cooperative estimate. The second belief consensus-based method further utilizes the symbol statistics provided during the EP iterations. Through iterative exchanges, distributed nodes collaboratively refine their beliefs and converge to a consistent and improved detection decision.

The remainder of this paper is organized as follows. Section II describes the baseband transmission procedure of the cooperative RSMA-AFDM system. In Section III, we analyze the diversity gain of cooperative RSMA-AFDM and accordingly formulate the objective of chirp parameter optimization. In Section IV, the optimization of chirp parameters for different users based on the goal of maximizing diversity gain is presented. Section V proposes a decision fusion-based detection algorithm and a belief consensus-based detection scheme for distributed cooperative RSMA-AFDM systems. We evaluate the performance of the proposed chirp parameter optimization and distributed cooperative detection algorithms for RSMA-AFDM through simulations in Section VI. Section VII concludes the paper.

II. COOPERATIVE RSMA-AFDM SYSTEM MODEL

In this section, we present the system model for the downlink cooperative RSMA-AFDM transmission. As shown in Fig. 1, at the base station, the transmitted symbols are first split into common streams and private streams. The common and private streams are then precoded in the DAFT domain and converted into time-domain signals using AFDM. At the receiver, the time-domain received signals are converted to the DAFT domain through AFDM demodulation.

Let N represent the number of symbols per frame. The transmitted symbol for User $k \in \{1, 2, \dots, K\}$ is expressed as \mathbf{X}_k , where K is the number of users. First, \mathbf{X}_k is divided into a common part $\mathbf{X}_{c,k}$ and a private part $\mathbf{X}_{p,k}$. The common parts of all users are concatenated into $\mathbf{X}_c = [\mathbf{X}_{c,1}^T, \mathbf{X}_{c,2}^T, \dots, \mathbf{X}_{c,K}^T]^T$ and precoded in the DAFT domain to obtain the common stream, where $(\cdot)^T$ is the matrix transpose. For simplicity in subsequent analysis, we set $\mathbf{X}_c \in \mathbb{C}^{N \times 1}$ and $\mathbf{X}_{p,k} \in \mathbb{C}^{N \times 1}$, where \mathbb{C} denotes the set of complex numbers. The private part of each user is individually precoded in the

DAFT domain. The final precoded DAFT domain transmitted symbols are expressed as

$$\mathbf{x} = \sqrt{\beta_c} \mathbf{w}_c \mathbf{X}_c + \sum_{k=1}^K \sqrt{\beta_{p,k}} \mathbf{w}_{p,k} \mathbf{X}_{p,k}, \quad (1)$$

where $\mathbf{x} = [\mathbf{x}_1^T, \mathbf{x}_2^T, \dots, \mathbf{x}_{N_t}^T]^T \in \mathbb{C}^{N_t N \times 1}$; N_t is the number of antennas; β_c and $\beta_{p,k}$ denote the power allocated to the common stream, and the private stream of User k , respectively, with $\beta_c + \sum_{k=1}^K \beta_{p,k} = 1$; $\mathbf{w}_c \in \mathbb{C}^{N_t N \times N}$ is the precoding matrix for the common stream; $\mathbf{w}_{p,k}$ represents the precoding matrix for the private stream of User k . Without loss of generality, we employ maximum ratio transmission (MRT) precoding for the common stream and zero forcing (ZF) precoding for the private streams [41]. The MRT precoding for the common stream is expressed as

$$\mathbf{w}_c = \frac{\sum_{k=1}^K \hat{\mathbf{H}}_k^\dagger}{\left\| \sum_{k=1}^K \hat{\mathbf{H}}_k^\dagger \right\|}, \quad (2)$$

where $\hat{\mathbf{H}}_k \in \mathbb{C}^{N \times N_t N}$ denotes the estimated DAFT domain equivalent channel of User k ; $(\cdot)^\dagger$ is the Hermitian operation; $\|\cdot\|$ is the Euclidean norm. The ZF precoding for the private streams needs to calculate the pseudo-inverse of matrix $\hat{\mathbf{H}} = [\hat{\mathbf{H}}_1^T, \hat{\mathbf{H}}_2^T, \dots, \hat{\mathbf{H}}_K^T]^T \in \mathbb{C}^{N K \times N_t N}$, which can be expressed as

$$\mathbf{D} = \frac{\hat{\mathbf{H}}^\dagger (\hat{\mathbf{H}} \hat{\mathbf{H}}^\dagger)^{-1}}{\left\| \hat{\mathbf{H}}^\dagger (\hat{\mathbf{H}} \hat{\mathbf{H}}^\dagger)^{-1} \right\|}. \quad (3)$$

User k 's private stream precoding matrix $\mathbf{w}_{p,k}$ is written as

$$\mathbf{w}_{p,k} = \mathbf{D}[:, (k-1)N : kN]. \quad (4)$$

Then, after reshaping DAFT domain transmitted symbols into $\mathbf{x} = [\mathbf{x}_1, \mathbf{x}_2, \dots, \mathbf{x}_{N_t}] \in \mathbb{C}^{N \times N_t}$, the inverse DAFT (IDAFT) is employed to convert \mathbf{x} to the time domain as

$$\mathbf{s} = \mathbf{A}^\dagger \mathbf{x} = \Lambda_{c_1}^\dagger \mathbf{F}^\dagger \Lambda_{c_2}^\dagger \mathbf{x}, \quad (5)$$

where $\mathbf{s} = [\mathbf{s}_1, \mathbf{s}_2, \dots, \mathbf{s}_{N_t}] \in \mathbb{C}^{N \times N_t}$ is the time-domain transmitted signal matrix; $\mathbf{A}^\dagger = \Lambda_{c_1}^\dagger \mathbf{F}^\dagger \Lambda_{c_2}^\dagger \in \mathbb{C}^{N \times N}$ is the IDAFT matrix; $\mathbf{F} \in \mathbb{C}^{N \times N}$ denotes the N -point DFT matrix with entries $e^{-j2\pi mn/N} / \sqrt{N}$; $\Lambda_{c_1} = \text{diag}(e^{-j2\pi c_1 n^2}, n =$

$0, 1, \dots, N-1$) and $\Lambda_{c_2} = \text{diag}(e^{-j2\pi c_2 n^2}, n = 0, 1, \dots, N-1)$; $\text{diag}(\mathbf{a})$ denotes a diagonal matrix whose main diagonal is \mathbf{a} ; c_1 and c_2 are AFDM parameters, where c_1 determines the slope of the chirps [9]. After inserting the chirp-periodic prefix (CPP), \mathbf{s} is transmitted to all users.

At the receiver, the time-domain received signal of User k can be expressed as

$$r_k[n] = \sum_{i=1}^{N_t} \sum_{l=0}^{\infty} s_i[n-l] \sum_{p=1}^P h_p^{[k,i]} e^{-j2\pi f_p^{[k,i]} n} \delta(l-l_p^{[k,i]}) + z_k[n], \quad (6)$$

where $\delta(\cdot)$ is the Dirac delta function; $h_p^{[k,i]}$, $f_p^{[k,i]}$, and $l_p^{[k,i]}$ represent the gain, Doppler shift index, and delay index of the p -th path from the i -th antenna to User k 's channel, respectively; P denotes the number of paths; $z_k[n]$ denotes the zero-mean complex additive white Gaussian noise (AWGN) with variance σ_k^2 . The matrix form of (6) can be expressed as

$$\mathbf{r}_k = \sum_{i=1}^{N_t} \mathbf{H}_T^{[k,i]} \mathbf{s}_i + \mathbf{z}_k, \quad (7)$$

where $\mathbf{H}_T^{[k,i]}$ denotes the time-domain equivalent channel from the i -th antenna to the k -th user.

The DAFT domain received symbol vector \mathbf{y}_k of User k can be expressed as

$$\mathbf{y}_k = \mathbf{A} \mathbf{r}_k = \Lambda_{c_2} \mathbf{F} \Lambda_{c_1} \mathbf{r}_k, \quad (8)$$

By stacking the received signals from the K users, we obtain

$$\mathbf{y} = \mathbf{H} \mathbf{x} + \mathbf{z}, \quad (9)$$

where $\mathbf{y} = [\mathbf{y}_1^T, \mathbf{y}_2^T, \dots, \mathbf{y}_K^T]^T \in \mathbb{C}^{NK \times 1}$; $\mathbf{x} = [\mathbf{x}_1^T, \mathbf{x}_2^T, \dots, \mathbf{x}_{N_t}^T]^T \in \mathbb{C}^{N_t N \times 1}$; $\mathbf{z} = [\mathbf{z}_1^T, \mathbf{z}_2^T, \dots, \mathbf{z}_K^T]^T \in \mathbb{C}^{NK \times 1}$; $\mathbf{H} \in \mathbb{C}^{NK \times N_t N}$ is the DAFT domain equivalent channel matrix and can be expressed as

$$\mathbf{H} = \begin{bmatrix} \mathbf{H}^{[1,1]} & \mathbf{H}^{[1,2]} & \dots & \mathbf{H}^{[1,N_t]} \\ \mathbf{H}^{[2,1]} & \mathbf{H}^{[2,2]} & \dots & \mathbf{H}^{[2,N_t]} \\ \vdots & \vdots & \ddots & \vdots \\ \mathbf{H}^{[K,1]} & \mathbf{H}^{[K,2]} & \dots & \mathbf{H}^{[K,N_t]} \end{bmatrix} \in \mathbb{C}^{NK \times N_t N}, \quad (10)$$

where

$$\mathbf{H}^{[k,i]} = \sum_{p=1}^P h_p^{[k,i]} \mathbf{A} \Gamma_{\text{CPP}_p^{[k,i]}} \Delta_{f_p^{[k,i]}} \mathbf{\Pi}^{l_p^{[k,i]}} \mathbf{A}^\dagger \quad (11)$$

denotes the DAFT domain equivalent channel from the i -th antenna to User k , where $\Delta_{f_p^{[k,i]}} \triangleq \text{diag}(e^{-j\frac{2\pi}{N} f_p^{[k,i]} n}, n = 0, 1, \dots, N-1) \in \mathbb{C}^{N \times N}$ is the spreading matrix induced by the Doppler shifts,

$$\Gamma_{\text{CPP}_p^{[k,i]}} = \text{diag} \left(\begin{cases} e^{-j2\pi c_1 (N^2 - 2N(l_p^{[k,i]} - n))} & n < l_p^{[k,i]} \\ 1 & n \geq l_p^{[k,i]} \end{cases} \right) \quad (12)$$

is the equivalent CPP matrix [19]; $\mathbf{\Pi} \in \mathbb{C}^{N \times N}$ represents the

forward cyclic shift matrix [42], given by

$$\mathbf{\Pi} = \begin{bmatrix} 0 & \dots & 0 & 1 \\ 1 & \dots & 0 & 0 \\ & \ddots & \ddots & \\ 0 & \dots & 1 & 0 \end{bmatrix}_{N \times N}. \quad (13)$$

In $\mathbf{H}^{[k,i]}$, each propagation path is represented by a cyclically shifted main diagonal; thus, $\mathbf{H}^{[k,i]}$ exhibits significant sparsity. Substituting (1) into (9), we have

$$\begin{aligned} \mathbf{y} &= \mathbf{H} (\sqrt{\beta_c} \mathbf{w}_c \mathbf{X}_c + \sum_{k=1}^K \sqrt{\beta_{p,k}} \mathbf{w}_{p,k} \mathbf{X}_{p,k}) + \mathbf{z} \\ &= \sqrt{\beta_c} \mathbf{G}_c \mathbf{X}_c + \sum_{k=1}^K \sqrt{\beta_{p,k}} \mathbf{G}_{p,k} \mathbf{X}_{p,k} + \mathbf{z}, \end{aligned} \quad (14)$$

where $\mathbf{G}_c = \mathbf{H} \mathbf{w}_c \in \mathbb{C}^{NK \times N}$ is the equivalent channel matrix of the common stream; $\mathbf{G}_{p,k} = \mathbf{H} \mathbf{w}_{p,k}$ is the equivalent channel matrix of the private stream of User k .

Next, the transmitted symbols need to be detected. The detection process consists of two steps. First, all user nodes cooperatively detect the common stream. Subsequently, each user eliminates the common stream components and independently detects the respective private streams. Since all users receive the same common stream, the cooperative RSMA-AFDM system can integrate broadcast information from other users to enhance the detection reliability through information fusion. Subsequently, using SIC scheme, the decoded common stream component is removed from the received signal. Finally, the private streams are detected. Given that ZF precoding is applied to the private streams, the receiver can recover the private streams using a simple linear equalization scheme. Ultimately, by combining the user-specific common stream portion with the private stream, the symbol detection is performed.

III. PERFORMANCE ANALYSIS

In this section, we analyze the performance of the proposed downlink cooperative RSMA-AFDM system, with a focus on the diversity gain when the users' channels are correlated. We focus on a two-user scenario [43], [44] representing a severe channel-correlation case, where both users share the same number of paths as well as identical delay and Doppler indices.

The system theoretical error performance is derived based on the PEP [9]. Given $K = 2$, the received signal in the DAFT domain for user k is expressed as

$$\begin{aligned} \mathbf{y}_k &= \sum_{i=1}^{N_t} \sqrt{\beta_c} \mathbf{G}_c^{[k,i]} \mathbf{X}_c + \\ &\underbrace{\sum_{i=1}^{N_t} (\sqrt{\beta_{p,1}} \mathbf{H}^{[k,i]} \mathbf{w}_p^{[1,i]} \mathbf{X}_{p,1} + \sqrt{\beta_{p,2}} \mathbf{H}^{[k,i]} \mathbf{w}_p^{[2,i]} \mathbf{X}_{p,2})}_{\boldsymbol{\psi}_k} + \mathbf{z}_k, \end{aligned} \quad (15)$$

where $\mathbf{w}_{c,i} \in \mathbb{C}^{N \times N}$; $\boldsymbol{\psi}_k$ represents the combined result of the interference terms.

To facilitate the PEP analysis, (15) is rewritten as

$$\begin{aligned} \mathbf{y}_k &= \sum_{i=1}^{N_t} \sum_{p=1}^P h_p^{[k,i]} \sqrt{\beta_c} \mathbf{G}_{c,p}^{[k,i]} \mathbf{X}_c + \psi_k \\ &= \sqrt{\beta_c} \sum_{i=1}^{N_t} (\Phi^{[k,i]}(\mathbf{X}_c) \mathbf{h}^{[k,i]} + \psi_k), \end{aligned} \quad (16)$$

and

$$\mathbf{h}^{[k,i]} = [h_1^{[k,i]}, h_2^{[k,i]}, \dots, h_P^{[k,i]}]^T \in \mathbb{C}^{P \times 1}, \quad (17)$$

and

$$\Phi^{[k,i]}(\mathbf{X}_c) = [\mathbf{G}_{c,1}^{[k,i]} \mathbf{X}_c, \mathbf{G}_{c,2}^{[k,i]} \mathbf{X}_c, \dots, \mathbf{G}_{c,P}^{[k,i]} \mathbf{X}_c] \in \mathbb{C}^{N \times P}. \quad (18)$$

We consider perfect channel state information (CSI) and employ maximum likelihood (ML) detection. At high signal-to-noise ratio (SNR), the conditional PEP of transmitting \mathbf{X}_c but decoding it as $\bar{\mathbf{X}}_c$ at the receiver is represented as

$$P(\mathbf{X}_c \rightarrow \bar{\mathbf{X}}_c) \leq \frac{1}{\left(\frac{1}{4N_0}\right)^R \prod_{d=1}^R \frac{\lambda_d^2}{P}}, \quad (19)$$

where N_0 represents the noise power; R is the exponent of the SNR term, which equals the rank of the matrix $\Phi^{[k,i]}(\delta)$ with $\delta = \mathbf{X}_c - \bar{\mathbf{X}}_c$; λ_d is the d -th singular value of the matrix $\Phi^{[k,i]}(\delta)$.

Therefore, the overall system error rate is dominated by the PEP corresponding to the smallest value of R .

The diversity order ρ of RSMA-AFDM is expressed as

$$\rho = \min_{\mathbf{X}_c \neq \bar{\mathbf{X}}_c} \text{rank}(\Phi^{[k,i]}(\delta)). \quad (20)$$

Ignoring the normalization term in (2) and substituting (2) into $\mathbf{G}_{c,p}^{[k,i]} = \mathbf{H}_p^{[k,i]} \mathbf{w}_{c,i,p}$, we obtain

$$\mathbf{G}_{c,p}^{[k,i]} = \mathbf{H}_p^{[k,i]} ((\mathbf{H}_p^{[1,i]})^\dagger + (\mathbf{H}_p^{[2,i]})^\dagger). \quad (21)$$

Without loss of generality, we let $k = 1$, and (21) can be further expressed as (22), which is provided at the bottom of this page.

To maximize the rank of the matrix $\Phi^{[1,i]}$, i.e., to achieve $\text{rank}(\Phi^{[1,i]}) = P$, it is necessary that, for each pair (p, q) with $p, q \in \{1, 2, \dots, P\}$, the vectors $\mathbf{H}_p^{[1,i]} ((\mathbf{H}_p^{[1,i]})^\dagger + (\mathbf{H}_p^{[2,i]})^\dagger) \mathbf{X}_c$ and $\mathbf{H}_q^{[1,i]} ((\mathbf{H}_q^{[1,i]})^\dagger + (\mathbf{H}_q^{[2,i]})^\dagger) \mathbf{X}_c$ are linearly independent. Since $l_p^{[1,i]} = l_p^{[2,i]}$ and $f_p^{[1,i]} = f_p^{[2,i]}$, we consider two users having the same AFDM chirp parameters (i.e., $c_{1,1} = c_{1,2}$, $c_{2,1} = c_{2,2}$), which implies that $\mathbf{H}^{[1,i]} = \mathbf{H}^{[2,i]}$. In this case, the necessary condition for maximizing the rank of $\Phi^{[1,i]}$ is: for each pair (p, q) , the $\mathbf{H}_p^{[1,i]} \mathbf{X}_c$ and $\mathbf{H}_q^{[1,i]} \mathbf{X}_c$ must be linearly independent. To achieve this, we adjust the parameter c_1 so that the paths in $\mathbf{H}^{[1,i]}$ do not overlap [9]. Furthermore, choosing c_2 to be irrational, we ensure that $\Phi^{[1,i]}(\mathbf{X}_c)$ has full rank, thereby obtaining the maximum diversity gain.

In the cooperative RSMA-AFDM system, each user can

broadcast its received signal to all other users. Consequently, the received signal at each user can be expressed as

$$\begin{aligned} \mathbf{y}_{co} &= \sum_{i=1}^{N_t} \sqrt{\beta_c} \mathbf{G}_{c,i} \mathbf{X}_c + \psi_i \\ &= \sqrt{\beta_c} \sum_{i=1}^{N_t} (\Phi_i(\mathbf{X}_c) \mathbf{h}_i + \psi_i), \end{aligned} \quad (23)$$

where $\mathbf{y}_{co} = [\mathbf{y}_1, \mathbf{y}_2]$; $\mathbf{G}_{c,i} = [\mathbf{G}_c^{[1,i]}, \mathbf{G}_c^{[2,i]}]$; $\psi_i = [\psi^{[1,i]}, \psi^{[2,i]}]$; $\mathbf{h}_i = [(\mathbf{h}^{[1,i]})^T, (\mathbf{h}^{[2,i]})^T]^T$; $\Phi_i(\mathbf{X}_c) = [\Phi^{[1,i]}(\mathbf{X}_c), \Phi^{[2,i]}(\mathbf{X}_c)]$ and can be expressed as

$$\Phi_i(\mathbf{X}_c) = [\mathbf{G}_{c,1}^{[1,i]} \mathbf{X}_c, \dots, \mathbf{G}_{c,P}^{[1,i]} \mathbf{X}_c, \mathbf{G}_{c,1}^{[2,i]} \mathbf{X}_c, \dots, \mathbf{G}_{c,P}^{[2,i]} \mathbf{X}_c]. \quad (24)$$

For common stream detection in cooperative RSMA-AFDM systems, a necessary condition for achieving the maximum diversity gain is that $\Phi_i(\mathbf{X}_c)$ has maximum rank. We have

$$\begin{aligned} \text{rank}(\Phi_i(\mathbf{X}_c)) &= \text{rank}(\Phi^{[1,i]}(\mathbf{X}_c)) + \text{rank}(\Phi^{[2,i]}(\mathbf{X}_c)) \\ &\quad - \text{rank}(\mathcal{C}(\Phi^{[1,i]}(\mathbf{X}_c)) \cap \mathcal{C}(\Phi^{[2,i]}(\mathbf{X}_c))), \end{aligned} \quad (25)$$

where $\mathcal{C}(\cdot)$ represents the column space of a matrix; $\mathcal{C}(\Phi^{[1,i]}(\mathbf{X}_c)) \cap \mathcal{C}(\Phi^{[2,i]}(\mathbf{X}_c))$ denotes the intersection of the column spaces of matrices $\Phi^{[1,i]}(\mathbf{X}_c)$ and $\Phi^{[2,i]}(\mathbf{X}_c)$. The upper and lower bounds of $\text{rank}(\Phi_i(\mathbf{X}_c))$ then follow as

$$\begin{aligned} \text{rank}(\Phi_i(\mathbf{X}_c)) &\leq \text{rank}(\Phi^{[1,i]}(\mathbf{X}_c)) + \text{rank}(\Phi^{[2,i]}(\mathbf{X}_c)), \\ \text{rank}(\Phi_i(\mathbf{X}_c)) &\geq \max \left\{ \text{rank}(\Phi^{[1,i]}(\mathbf{X}_c)), \text{rank}(\Phi^{[2,i]}(\mathbf{X}_c)) \right\}. \end{aligned} \quad (26)$$

When the column spaces of $\Phi^{[1,i]}(\mathbf{X}_c)$ and $\Phi^{[2,i]}(\mathbf{X}_c)$ are linearly independent, the system operates at its performance upper bound. In contrast, as the correlation between these column spaces increases, the performance approaches its lower bound. Therefore, to achieve the maximum diversity gain, in addition to guaranteeing that $\Phi^{[1,i]}(\mathbf{X}_c)$ and $\Phi^{[2,i]}(\mathbf{X}_c)$ are full rank, it is also desirable to minimize the correlation between their column spaces. Implementing these conditions requires that the paths in $\mathbf{H}^{[1,i]}$ and $\mathbf{H}^{[2,i]}$ do not overlap and that the paths associated with $\mathbf{H}^{[1,i]}$ and $\mathbf{H}^{[2,i]}$ are mutually orthogonal. Moreover, minimizing the overlap between these column spaces leads to a minimal correlation between $\mathbf{H}^{[1,i]}$ and $\mathbf{H}^{[2,i]}$, which in turn minimizes the interference among the private streams of different users.

The above conclusion can be directly extended to the scenarios with $K \geq 3$. Specifically, when the overlap among the DAFT-domain equivalent-channel column spaces of all users is minimized, the channel correlation is reduced to its lowest level and the cooperative RSMA-AFDM system attains the maximum diversity gain.

IV. AFDM CHIRP PARAMETER OPTIMIZATION

In this section, we first construct an optimization problem aimed at maximizing cooperative diversity gain. The core

$$\Phi^{[1,i]}(\mathbf{X}_c) = [(\mathbf{H}_1^{[1,i]} ((\mathbf{H}_1^{[1,i]})^\dagger + (\mathbf{H}_1^{[2,i]})^\dagger)) \mathbf{X}_c, (\mathbf{H}_2^{[1,i]} ((\mathbf{H}_2^{[1,i]})^\dagger + (\mathbf{H}_2^{[2,i]})^\dagger)) \mathbf{X}_c, \dots, (\mathbf{H}_P^{[1,i]} ((\mathbf{H}_P^{[1,i]})^\dagger + (\mathbf{H}_P^{[2,i]})^\dagger)) \mathbf{X}_c]. \quad (22)$$

objective is to minimize the overlap among the channel paths of different users, subject to the constraint that the paths of each user do not overlap. Building on this, we propose a method to solve the optimization problem by adjusting the AFDM chirp parameters. We also provide a chirp parameter configuration scheme that achieves the maximum diversity gain of cooperative RSMA-AFDM systems.

A. Problem Formulation

$H^{[k,i]}[r, t]$ is expressed as

$$H^{[k,i]}[r, t] = e^{j2\pi c_2(t^2 - r^2)} e^{-j\frac{2\pi}{N}((r-1) + f_p^{[k,i]} + (l_p^{[k,i]} + 1)(t-1))} \times \sum_{n=0}^{N-1} e^{-j\frac{2\pi}{N}n(2Nl_p^{[k,i]}c_1 + r + f_p^{[k,i]} - t)}. \quad (27)$$

Let $\mathcal{F}_p(r, t) = \sum_{n=0}^{N-1} e^{-j\frac{2\pi}{N}n(2Nl_p^{[k,i]}c_1 + r + f_p^{[k,i]} - t)}$, and we have

$$\mathcal{F}_p(r, t) = \frac{1 - e^{-j2\pi(r-t+2Nl_p^{[k,i]}c_1 + f_p^{[k,i]})}}{1 - e^{-j\frac{2\pi}{N}(r-t+2Nl_p^{[k,i]}c_1 + f_p^{[k,i]})}}. \quad (28)$$

For simplicity, let $\text{loc}_p^{[k,i]} = (f_p^{[k,i]} + 2Nc_1l_p^{[k,i]})_N$. When only integer Doppler shift is considered, $H^{[k,i]}[r, t]$ is non-zero only if $t = r + \text{loc}_p^{[k,i]}$ [9].

Here, the correlation between user equivalent channels is reduced by adjusting the AFDM chirp parameters for different users. We also consider a two-user scenario that represents a severe channel-correlation case, where the two users have the same number of paths as well as identical delay and Doppler indices.

The structure of $\mathbf{H}_i = [(\mathbf{H}^{[1,i]})^T, (\mathbf{H}^{[2,i]})^T]^T$ is shown in Fig. 2. The optimization objective is to ensure that the paths in the DAFT-domain equivalent channel $\mathbf{H}^{[k,i]}$ do not overlap, while making the overlap between the paths of $\mathbf{H}^{[1,i]}$ and $\mathbf{H}^{[2,i]}$ to be minimized, thereby achieving the maximum rank. Meanwhile, the periodic aliasing in the DAFT-domain channels must be avoided. Therefore, the optimization problem can be formulated as

$$\min \sum_{p=1}^P \sum_{q=1}^P \mathbb{I}(\text{loc}_p^{[2,i]} = \text{loc}_q^{[1,i]}) \quad (29a)$$

$$\text{s.t. } \text{loc}_p^{[k,i]} \neq \text{loc}_q^{[k,i]}, \quad \forall p, q \in \{1, \dots, P\}, p \neq q \quad (29b)$$

$$|\text{loc}_p^{[2,i]} - \text{loc}_q^{[1,i]}| < N, \quad \forall p, q \in \{1, \dots, P\}, \quad (29c)$$

where $\mathbb{I}(\text{loc}_p^{[2,i]} = \text{loc}_q^{[1,i]})$ is 1 if $\text{loc}_p^{[2,i]} = \text{loc}_q^{[1,i]}$, and 0 otherwise. We will elaborate this optimization problem in subsection B.

B. Optimal Chirp Parameters

We consider the values of $f_p^{[k,i]}$ and $f_q^{[k,i]}$ for the two users in the range $[-f_{\max}, f_{\max}]$, and the values of $l_p^{[k,i]}$ and $l_q^{[k,i]}$ in the range $[0, l_{\max}]$. For the condition in (29b), given $f_p^{[k,i]} > f_q^{[k,i]}$, it should satisfy

$$\forall p, q \in \{1, \dots, P\} \quad \text{and} \quad p \neq q, \quad \text{loc}_p^{[k,i]} > \text{loc}_q^{[k,i]}. \quad (30)$$

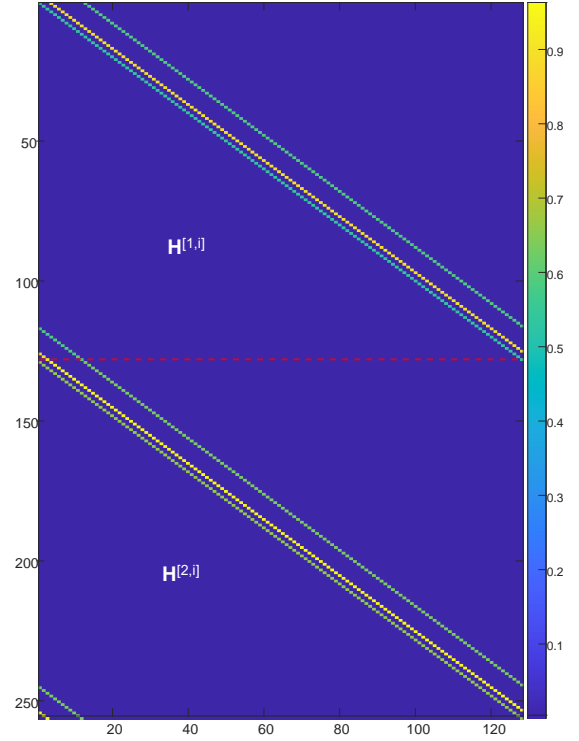


Fig. 2. The structure of DAFT domain equivalent channels for two users.

By substituting $\text{loc}_p^{[k,i]} = f_p^{[k,i]} + 2Nc_1l_p^{[k,i]}$ and $\text{loc}_q^{[k,i]} = f_q^{[k,i]} + 2Nc_1l_q^{[k,i]}$, into (30), the condition can be rewritten as

$$c_1 > \frac{f_p^{[k,i]} - f_q^{[k,i]}}{2N(l_p^{[k,i]} - l_q^{[k,i]})}, \quad (31)$$

where $f_p^{[k,i]} - f_q^{[k,i]} \leq 2f_{\max}$, and since fractional delay index is not considered, we have $l_p^{[k,i]} - l_q^{[k,i]} \geq 1$. Therefore, the minimum value of c_1 that guarantees no overlap among all paths of $\mathbf{H}^{[k,i]}$ is

$$c_1 = \frac{2f_{\max} + 1}{2N}. \quad (32)$$

By choosing c_2 as an irrational number, the paths in $\mathbf{H}^{[k,i]}$ are uncorrelated, which guarantees that $\Phi^{[k,i]}(\mathbf{X}_c)$ attains its maximum rank [9].

To solve the optimization problem in (29), our approach is to assign different values of c_1 to the two users. Without loss of generality, we allocate $c_{1,1} = \frac{2f_{\max} + 1}{2N}$ to User 1, which is the minimum value that can distinguish different propagation paths. For User 2, our objective is to minimize the overlap of its paths with those of User 1. This is achieved by increasing the value of $c_{1,2}$ to increase $\text{loc}_p^{[2,i]}$, thereby maximizing the possibility of realizing

$$\text{loc}_p^{[2,i]} > \text{loc}_q^{[1,i]}, \quad \forall p, q \in \{1, \dots, P\}. \quad (33)$$

To achieve this, it is necessary to satisfy $\text{loc}_{\min}^{[2,i]} > \text{loc}_{\max}^{[1,i]}$, where

$$\text{loc}_{\max}^{[1,i]} = f_{\max} + 2Nc_{1,1}l_{\max}. \quad (34)$$

We use $c_{1,2}$ to denote the parameter c_1 for User 2. Note that when $l_p^{[2,i]} = 0$, the $\text{loc}_p^{[2,i]}$ of this path cannot be changed

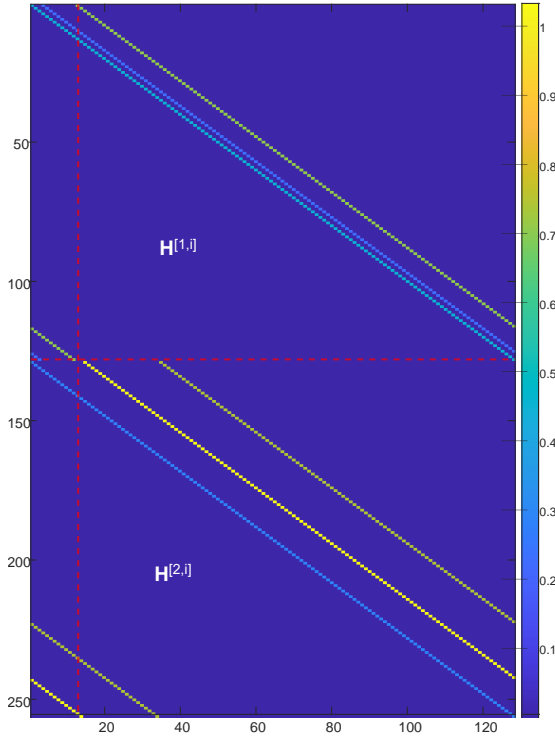


Fig. 3. The DAFT domain equivalent channels for two users with the optimized chirp parameters.

by adjusting c_1 . In such cases, the correlation can be reduced by adjusting the value of c_2 . Therefore, $\text{loc}_{\min}^{[2,i]}$ is expressed as

$$\text{loc}_{\min}^{[2,i]} = -f_{\max} + 2Nc_{1,2}, \quad (35)$$

The inequality $\text{loc}_p^{[2,i]} > \text{loc}_q^{[1,i]}$ can be further derived as

$$c_{1,2} > \frac{f_{\max}}{N} + c_{1,1}l_{\max}. \quad (36)$$

Remark 1: If considering $K \geq 3$, the corresponding condition becomes

$$c_{1,k+1} > \frac{f_{\max}}{N} + c_{1,k}l_{\max} \quad (37)$$

should be satisfied to ensure minimal channel correlation among all users.

Substituting the value of $c_{1,1}$, (36) can be further expressed as

$$c_{1,2} > \frac{2f_{\max} + 2f_{\max}l_{\max} + l_{\max}}{2N}. \quad (38)$$

Therefore, the minimum value of $c_{1,2}$ set to ensure the lowest correlation between two user channels is

$$c_{1,2} = \frac{2f_{\max} + 2f_{\max}l_{\max} + l_{\max} + 1}{2N}. \quad (39)$$

The structure of $\mathbf{H}_i = [(\mathbf{H}^{[1,i]})^T, (\mathbf{H}^{[2,i]})^T]^T$ with the optimized c_1 value is shown in Fig. 3. Since c_1 cannot change the position of the path with $l_p^{[k,i]} = 0$ in the DAFT domain equivalent channel, the correlation between the channels can only be reduced by adjusting the value of c_2 . Except for the path with $l_p^{[k,i]} = 0$, the proposed c_1 optimization method effectively avoids path overlap between the channels of two

users, thereby enhancing cooperative diversity gain.

Meanwhile, to avoid the periodic aliasing in (29c), we need to ensure that

$$2f_{\max} + (2f_{\max} + 2f_{\max}l_{\max} + l_{\max} + 1)l_{\max} < N. \quad (40)$$

This is easily achievable in wireless communication system.

If considering fractional Doppler shifts, (36) becomes

$$c_{1,2} > \frac{f_{\max} + \xi_f}{N} + c_{1,1}l_{\max}, \quad (41)$$

and

$$c_{1,1} = \frac{2f_{\max} + 2\xi_f + 1}{2N}. \quad (42)$$

Thus, the value of $c_{1,2}$ is expressed as

$$c_{1,2} = \frac{2f_{\max} + 2\xi_f + 2f_{\max}l_{\max} + 2\xi_f l_{\max} + l_{\max} + 1}{2N}, \quad (43)$$

where ξ_f is the guard bandwidth to avoid fractional Doppler-induced overlap.

The proposed method exploits the flexibility of chirp parameter design in AFDM. By assigning different chirp parameters to different users, it significantly reduces the correlation among the DAFT-domain equivalent channels and thereby improves the available diversity gain of the cooperative RSMA-AFDM system.

V. DISTRIBUTED COOPERATIVE EP DETECTION

To fully exploit the cooperative diversity gain by adjusting the chirp parameters of different users, the design of cooperative detection algorithms is crucial. This section focuses on the distributed common stream detection algorithms in cooperative RSMA-AFDM systems. First, we introduce a decision fusion EP-based method for common stream detection. This scheme leverages a distributed cooperative framework in which each user performs local EP detection, and then combines its local result with the information broadcast by other users via MRC. Subsequently, we elaborate on the further-designed belief consensus EP-based distributed cooperative method. Through multiple rounds of distributed exchange and integration of information among cooperating users, the adverse impact of the private stream components on the accuracy of prior information is effectively mitigated. As a result, all distributed nodes gradually converge to a consistent and improved decision under the belief consensus-based scheme.

A. EP-Based Decision Fusion

In this subsection, we present the decision fusion EP-based detection algorithm for the downlink cooperative RSMA-AFDM system. This method introduces a distributed cooperative mechanism in which the users broadcast their local detection results and fuse the information received from other nodes. Specifically, each user first performs local EP detection on the received signal and then broadcasts the detection result to the other users. Subsequently, all users combine their local EP detection output with the information broadcast by other users using MRC, thereby achieving reliable demodulation of the common stream.

The received signal in the DAFT domain for user k can be expressed as

$$\mathbf{y}_k = \sqrt{\beta_c} \mathbf{G}_{c,k} \mathbf{X}_c + \boldsymbol{\psi}_k, \quad (44)$$

where $\mathbf{G}_{c,k} = \mathbf{H}_k \mathbf{w}_c \in \mathbb{C}^{N \times N}$ is the equivalent channel of User k .

The *a posteriori* probability distribution of the DAFT domain transmitted symbols \mathbf{X}_c can be expressed as

$$p(\mathbf{X}_c | \mathbf{y}_k) \propto \underbrace{\mathcal{N}(\mathbf{y}_k; \mathbf{G}_{c,k} \mathbf{X}_c, \sigma_c^2 \mathbf{I}_N)}_{p(\mathbf{y}_k | \mathbf{X}_c)} \underbrace{\prod_{m=1}^N p(X_c[m])}_{p(\mathbf{X}_c)}, \quad (45)$$

where \mathbf{I}_N denotes the $N \times N$ identity matrix. $p(\mathbf{X}_c)$ represents the *a priori* distribution of $\mathbf{X}_c[m]$, which is denoted as

$$p(\mathbf{X}_c) = \prod_{m=1}^N \mathbb{I}(X_c[m] \in \mathcal{A}), \quad (46)$$

where \mathcal{A} is the modulation constellation set.

Since $p(\mathbf{X}_c)$ is not Gaussian, computing $p(\mathbf{X}_c | \mathbf{y}_k)$ directly would require traversing all possible values of \mathbf{X}_c , which results in exponential complexity and makes practical implementation prohibitive [45]. Therefore, we employ the EP algorithm to approximate the solution to $p(\mathbf{X}_c | \mathbf{y}_k)$. The EP detection algorithm provides approximate ML solutions while significantly reducing the computational complexity. EP constructs a simple Gaussian distribution $q(\mathbf{X}_c)$ to approximate $p(\mathbf{X}_c | \mathbf{y}_k)$. Through moment matching, EP enables the statistical properties of the constructed $q(\mathbf{X}_c)$ closely align with those of $p(\mathbf{X}_c)$, thereby supporting detection performance.

The received symbol vector \mathbf{y}_k , as shown in (44), can be transformed into a real-valued symbol representation as

$$\tilde{\mathbf{y}}_k = \sqrt{\beta_c} \tilde{\mathbf{G}}_{c,k} \tilde{\mathbf{X}}_c + \tilde{\boldsymbol{\psi}}_k, \quad (47)$$

where

$$\begin{aligned} \tilde{\mathbf{y}}_k &= [\mathcal{R}\{\mathbf{y}_k\}^T \quad \mathcal{I}\{\mathbf{y}_k\}^T]^T \in \mathbb{R}^{2N \times 1}, \\ \tilde{\mathbf{X}}_c &= [\mathcal{R}\{\mathbf{X}_c\}^T \quad \mathcal{I}\{\mathbf{X}_c\}^T]^T \in \mathbb{R}^{2N \times 1}, \\ \tilde{\boldsymbol{\psi}}_k &= [\mathcal{R}\{\boldsymbol{\psi}_k\}^T \quad \mathcal{I}\{\boldsymbol{\psi}_k\}^T]^T \in \mathbb{R}^{2N \times 1}, \\ \tilde{\mathbf{G}}_{c,k} &= \begin{bmatrix} \mathcal{R}\{\mathbf{G}_{c,k}\} & -\mathcal{I}\{\mathbf{G}_{c,k}\} \\ \mathcal{I}\{\mathbf{G}_{c,k}\} & \mathcal{R}\{\mathbf{G}_{c,k}\} \end{bmatrix} \in \mathbb{R}^{2N \times 2N}, \end{aligned} \quad (48)$$

where \mathbb{R} signifies the set of real numbers; $\mathcal{R}(\mathbf{a})$ and $\mathcal{I}(\mathbf{a})$ denote the real and imaginary parts, respectively.

Then $q(\tilde{\mathbf{X}}_c) = \prod_{n=1}^{2N} e^{\gamma_n^{(l)} \tilde{X}_c[n] - \frac{1}{2} \lambda_n^{(l)} \tilde{X}_c[n]^2}$ is constructed to replace the original *a priori* distribution $p(\tilde{\mathbf{X}}_c)$, where $\gamma_n^{(l)}$ and $\lambda_n^{(l)}$ denote two parameters that are iteratively updated to achieve a more accurate approximation of the true distribution; l is the EP iteration index.

Both $p(\tilde{\mathbf{y}}_k | \tilde{\mathbf{X}}_c)$ and $q^{(l)}(\tilde{\mathbf{X}}_c)$ follow Gaussian distributions, such that their product $p^{(l)}(\tilde{\mathbf{X}}_c | \tilde{\mathbf{y}}_k)$ also follows a Gaussian distribution. Through theoretical derivation, we have $p^{(l)}(\tilde{\mathbf{X}}_c | \tilde{\mathbf{y}}_k) \propto \mathcal{N}(\tilde{\mathbf{X}}_c; \boldsymbol{\mu}^{(l)}, \boldsymbol{\Sigma}^{(l)})$, whose explicit expression is given by

$$\begin{aligned} \boldsymbol{\Sigma}^{(l)} &= \left(\sigma_c^{-2} \tilde{\mathbf{G}}_{c,k}^T \tilde{\mathbf{G}}_{c,k} + \text{diag}\{\boldsymbol{\lambda}^{(l-1)}\} \right)^{-1}, \\ \boldsymbol{\mu}^{(l)} &= \sigma_c^{-2} \boldsymbol{\Sigma}^{(l)} \tilde{\mathbf{G}}_{c,k}^T \tilde{\mathbf{y}}_k + \boldsymbol{\Sigma}^{(l)} \boldsymbol{\gamma}^{(l-1)}, \end{aligned} \quad (49)$$

where $\boldsymbol{\lambda}^{(l-1)} = [\lambda_1^{(l-1)}, \dots, \lambda_{2N}^{(l-1)}]^T \in \mathbb{R}^{2N \times 1}$; $\boldsymbol{\mu}^{(l)} = [\mu_1^{(l)}, \dots, \mu_{2N}^{(l)}]^T \in \mathbb{R}^{2N \times 1}$; $\boldsymbol{\gamma}^{(l-1)} = [\gamma_1^{(l-1)}, \dots, \gamma_{2N}^{(l-1)}]^T \in \mathbb{R}^{2N \times 1}$; $\boldsymbol{\Sigma}^{(l)} = \text{diag}([\Sigma_1^{(l)}, \dots, \Sigma_{2N}^{(l)}]) \in \mathbb{R}^{2N \times 2N}$.

Given the independence of transmitted symbols, the joint distribution factorizes into individual components, each representing the distribution of a single symbol, which is given by

$$p^{(l)}(\tilde{\mathbf{X}}_c | \tilde{\mathbf{y}}_k) = \prod_{n=1}^{2N} \underbrace{\mathcal{N}(\tilde{X}_c[n]; \mu_n^{(l)}, \Sigma_n^{(l)})}_{p^{(l)}(\tilde{X}_c[n] | \tilde{\mathbf{y}}_k)}. \quad (50)$$

Next, the DAFT-domain cavity distribution [46] is obtained by dividing $p^{(l)}(\tilde{X}_c[n] | \tilde{\mathbf{y}}_k)$ by $q^{(l)}(\tilde{X}_c[n])$, which can be expressed as

$$p^{(l) \setminus n}(\tilde{X}_c[n] | \tilde{\mathbf{y}}_k) \triangleq \frac{p^{(l)}(\tilde{X}_c[n] | \tilde{\mathbf{y}}_k)}{q^{(l)}(\tilde{X}_c[n])} \propto \mathcal{N}(\tilde{X}_c[n]; E_n^{(l)}, \varepsilon_n^{(l)}), \quad (51)$$

where

$$\begin{aligned} \varepsilon_n^{(l)} &= \frac{\Sigma_n^{(l)}}{1 - \Sigma_n^{(l)} \lambda_n^{(l-1)}}, \\ E_n^{(l)} &= \varepsilon_n^{(l)} \left(\frac{\mu_n^{(l)}}{\Sigma_n^{(l)}} - \gamma_n^{(l-1)} \right). \end{aligned} \quad (52)$$

Then, it is necessary to calculate the moments of $p^{(l) \setminus n}(\tilde{X}_c[n] | \tilde{\mathbf{y}}_k) p(\tilde{X}_c[n])$. Given the random nature of the transmitted signal, $p(\tilde{X}_c[n])$ may be regarded as a uniform distribution over the space of constellation points. The first-order moment $\chi_n^{(l)}$ and second-order moment $C_n^{(l)}$ can be computed as

$$\begin{aligned} \chi_n^{(l)} &= \sum_{a \in \tilde{\mathcal{A}}} a \times q^{(l) \setminus n}(\tilde{X}_c[n] = a), \\ C_n^{(l)} &= \sum_{a \in \tilde{\mathcal{A}}} (a - \chi_n^{(l)})^2 \times q^{(l) \setminus n}(\tilde{X}_c[n] = a). \end{aligned} \quad (53)$$

where $\tilde{\mathcal{A}}$ is the set of real-valued constellation points. Then, moment matching is performed between $p^{(l) \setminus n}(\tilde{X}_c[n] | \tilde{\mathbf{y}}_k) p(\tilde{X}_c[n])$ and $p^{(l) \setminus n}(\tilde{X}_c[n] | \tilde{\mathbf{y}}_k) q^{(l)}(\tilde{X}_c[n])$ to update the parameters of $q^{(l)}(\tilde{X}_c[n])$ as

$$\begin{aligned} \boldsymbol{\lambda}^{(l)} &= (\mathbf{C}^{(l)})^{-1} - (\boldsymbol{\varepsilon}^{(l)})^{-1}, \\ \boldsymbol{\gamma}^{(l)} &= (\mathbf{C}^{(l)})^{-1} \boldsymbol{\chi}^{(l)} - (\boldsymbol{\varepsilon}^{(l)})^{-1} \mathbf{E}^{(l)}, \end{aligned} \quad (54)$$

where $\mathbf{C}^{(l)} = \text{diag}([C_1^{(l)}, \dots, C_{2N}^{(l)}]) \in \mathbb{R}^{2N \times 2N}$; $\boldsymbol{\chi}^{(l)} = [\chi_1^{(l)}, \dots, \chi_{2N}^{(l)}]^T \in \mathbb{R}^{2N \times 1}$; $\boldsymbol{\varepsilon}^{(l)} = \text{diag}([\varepsilon_1^{(l)}, \dots, \varepsilon_{2N}^{(l)}]) \in \mathbb{R}^{2N \times 2N}$; $\mathbf{E}^{(l)} = [E_1^{(l)}, \dots, E_{2N}^{(l)}]^T \in \mathbb{R}^{2N \times 1}$.

Finally, a damping parameter η is employed to control the convergence rate, which can be expressed as

$$\begin{aligned} \boldsymbol{\lambda}^{(l)} &= (1 - \eta) \boldsymbol{\lambda}^{(l-1)} + \eta \boldsymbol{\lambda}^{(l)}, \\ \boldsymbol{\gamma}^{(l)} &= (1 - \eta) \boldsymbol{\gamma}^{(l-1)} + \eta \boldsymbol{\gamma}^{(l)}. \end{aligned} \quad (55)$$

The above steps are iterated until either the preset maximum number of iterations L is reached or the target accuracy is achieved.

After each user performs EP detection on the common data stream locally, it broadcasts the detection result χ_k to other users. Subsequently, all users fuse the local EP

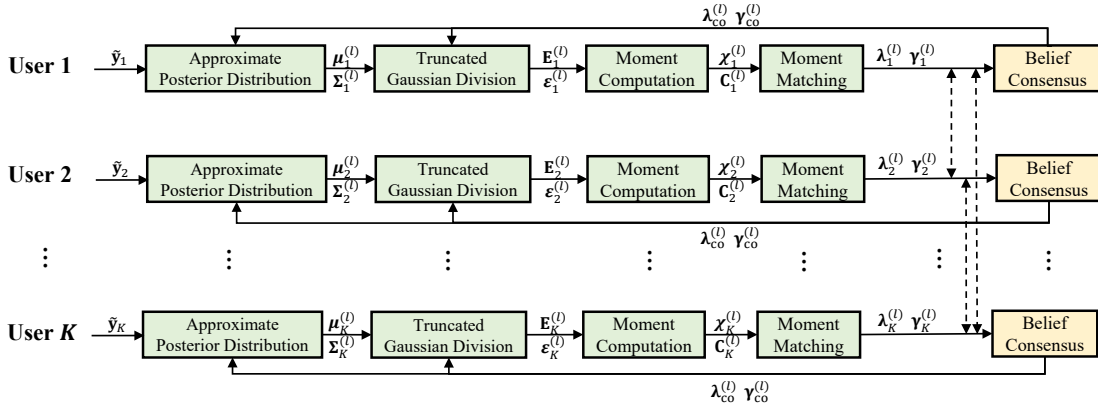


Fig. 4. Illustration of the belief consensus-based cooperative EP detection.

detection output expectation χ_k with the cooperative information $\chi_v (v = 1, \dots, K, v \neq k)$ received from neighboring users to achieve a consistent estimate of the global message. Specifically, under the assumption that the channel gains are normalized, this fusion process is implemented by performing MRC on the information from multiple nodes, expressed as

$$\chi_{co}^{(L)} = \sum_{v=1}^K \frac{\sigma_v^{-2}}{\sum_{j=1}^K \sigma_j^{-2}} \chi_v^{(L)}. \quad (56)$$

By this method, each signal is weighted according to its SNR, allowing the system to significantly optimize the overall output quality during the signal merging process, thereby maximizing the SNR gain.

B. EP-Based Belief Consensus

In the RSMA-AFDM system, although the decision fusion EP-based cooperative detection scheme achieves diversity gain, its performance is limited because it does not fully exploit the information generated during the EP iterations. Furthermore, during the detection of the common stream in the RSMA-AFDM system, interference includes not only AWGN but also private stream components, which compromises the accuracy of the noise variance prior information used by the current EP detector. Unfortunately, this decision fusion-based cooperative detection mechanism fails to effectively enhance the accuracy of noise variance information through node collaboration, as it only obtains cooperative diversity gain by merging the final expectation term $\chi^{(L)}$.

To further enhance the detection performance of common data streams in the system, we introduce a belief consensus-based EP detection algorithm for cooperative RSMA-AFDM system, as shown in Fig. 4. This algorithm allows each node to iteratively exchange and update its beliefs regarding the common stream information with neighboring nodes over multiple rounds, gradually achieving globally consistent detection results in the distributed network.

In each round of EP iteration, each user node outputs the parameters $\lambda^{(l)}$ and $\gamma^{(l)}$ of its local $q^{(l)}(\tilde{\mathbf{X}}_c)$. Subsequently, the system performs belief consensus operations on these parameters. Specifically, each user recursively updates its own

Algorithm 1 The belief consensus-based distributed cooperative detection for common stream in RSMA-AFDM.

Input: $\tilde{\mathbf{y}}, \tilde{\mathbf{G}}_c$, mean symbol energy E_s, L, σ^2 .

Initial: $\gamma_n = 0, \lambda_n = E_s^{-1}$.

- 1: **for** $l = 1 : L$ **do**
- 2: Compute $\Sigma_n^{(l)}$ and $\mu_n^{(l)}$ by (49);
- 3: Compute $\varepsilon_n^{(l)}$ and $E_n^{(l)}$ by (52);
- 4: Compute $\chi_n^{(l)}$ and $C_n^{(l)}$ by (53);
- 5: Compute $\lambda_n^{(l)}$ and $\gamma_n^{(l)}$ by (54);
- 6: Update $\lambda_n^{(l)}$ and $\gamma_n^{(l)}$ by (55);
- 7: Compute $\lambda_{co,n}^{(l)}$ and $\gamma_{co,n}^{(l)}$ by (57);
- 8: Set $\lambda_n^{(l)} = \lambda_{co,n}^{(l)}, \gamma_n^{(l)} = \gamma_{co,n}^{(l)}$;
- 9: **end for**
- 10: Eliminate the common stream component by (58);
- 11: Detect the private stream by (61);
- 12: **return** $\tilde{\mathbf{X}}$.

local belief according to the MRC-based belief consensus rule, which can be expressed as

$$\begin{aligned} \lambda_{co}^{(l)} &= \sum_{v=1}^K \frac{\sigma_v^{-2}}{\sum_{j=1}^K \sigma_j^{-2}} \lambda_v^{(l)}, \\ \gamma_{co}^{(l)} &= \sum_{v=1}^K \frac{\sigma_v^{-2}}{\sum_{j=1}^K \sigma_j^{-2}} \gamma_v^{(l)}. \end{aligned} \quad (57)$$

Subsequently, each user node utilizes $\lambda_{co}^{(l)}$ and $\gamma_{co}^{(l)}$ in the $(l+1)$ -th EP iteration.

This belief consensus-based cooperative strategy not only reduces the risk of bit errors caused by poor channel conditions at individual nodes but also enhances the system robustness against channel fluctuations and interference. Owing to the different channel conditions experienced by users in the downlink, the multi-user distributed cooperative detection scheme fully exploits spatial and cooperative diversity gain, thereby improving system reliability and demonstrating clear advantages over traditional non-cooperative detection methods. Moreover, the chirp parameter optimization proposed in Section IV reduces the channel correlation among users. Building on this benefit, the proposed belief consensus-based cooperative detection algorithm can further leverage its advantages,

thereby achieving higher detection performance and effectively enhancing the overall reliability.

After detecting the common stream, its component is removed from the received signal \mathbf{y}_k as

$$\hat{\mathbf{y}}_{p,k} = \mathbf{y}_k - \sqrt{\beta_c} \mathbf{G}_{c,k} \hat{\mathbf{X}}_c, \quad (58)$$

where $\hat{\mathbf{X}}_c$ represents the common stream estimated by the proposed cooperative detection scheme; $\hat{\mathbf{y}}_{p,k}$ denotes the private stream component obtained after SIC. Assuming perfect common stream estimation, $\hat{\mathbf{y}}_{p,k}$ is expressed as

$$\hat{\mathbf{y}}_{p,k} = \mathbf{H}_k \sum_{v=1}^K \sqrt{\beta_{p,v}} \mathbf{w}_{p,v} \mathbf{X}_{p,v} + \mathbf{z}_k. \quad (59)$$

When the channels of different users are uncorrelated, inter-user interference is cancelled by ZF precoding, and $\hat{\mathbf{y}}_{p,k}$ becomes

$$\hat{\mathbf{y}}_{p,k} = \sqrt{\beta_{p,k}} \mathbf{H}_k \mathbf{w}_{p,k} \mathbf{X}_{p,k} + \mathbf{z}_k = \sqrt{\beta_{p,k}} \mathbf{G}_{p,k} \mathbf{X}_{p,k} + \mathbf{z}_k, \quad (60)$$

where $\mathbf{G}_{p,k}$ denotes the equivalent channel matrix of the private stream for the k -th user, which is approximated by a diagonal matrix. The private stream is detected using minimum mean square error (MMSE), yielding

$$\hat{\mathbf{X}}_{p,k} = (\mathbf{G}_{p,k}^\dagger \mathbf{G}_{p,k} + \sigma_k^2 \mathbf{I}_N)^{-1} \mathbf{G}_{p,k}^\dagger \hat{\mathbf{y}}_{p,k} / \sqrt{\beta_{p,k}}. \quad (61)$$

The detailed process of the proposed cooperative RSMA-AFDM detection is described in Algorithm 1. Since $\mathbf{G}_{p,k}$ is approximately diagonal, the complexity of private stream detection is low. Additionally, the proposed belief consensus-based cooperative detection scheme accurately recovers the common stream, whereas the chirp parameter optimization in Section IV effectively reduces the correlation among different users' channels, thereby enabling reliable detection of the private streams.

VI. SIMULATION RESULTS

In this section, we demonstrate the performance gain provided by the proposed chirp parameter optimization for the RSMA-AFDM system and the cooperative detectors through simulations. We also evaluate the proposed decision-fusion cooperative detection scheme and the belief consensus-based cooperative EP detection scheme. The conventional MMSE, EP [15], Gaussian message passing (GMP) [47], and iterative MMSE (I-MMSE) [48] are used as benchmarks. We consider a downlink RSMA-AFDM system with two users. The power allocation factor for the common stream is $p_c = 0.75$. The number of symbols per AFDM frame is set to $N = 64$, the number of paths is $P = 4$, with maximum delay index $l_{\max} = 2$ and maximum Doppler index $f_{\max} = 2$. The chirp parameter $c_{1,1}$ for User 1 is set to $\frac{2f_{\max} + 2\xi_f + 1}{2N}$, and $c_{1,2}$ for User 2 is chosen as $\frac{2f_{\max} + 2\xi_f + 2f_{\max}l_{\max} + 2\xi_f l_{\max} + l_{\max} + 1}{2N}$, where $\xi_f = 1$. Additionally, the parameters $c_{2,1}$ and $c_{2,2}$ are selected as distinct irrational numbers. Specifically, in our simulations, we set $c_{2,1} = \frac{1}{N\pi}$ and $c_{2,2} = \frac{1}{N^2\pi}$.

Here, we simulate the BER performance of the RSMA-AFDM system and evaluate the performance improvement provided by the proposed chirp parameter optimization

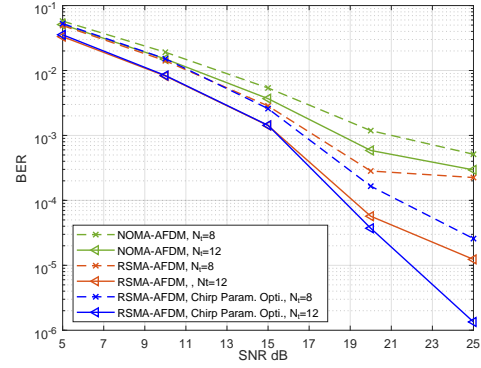


Fig. 5. BER vs. SNR for the chrip-optimized RSMA-AFDM and NOMA-AFDM in non-cooperative communications.

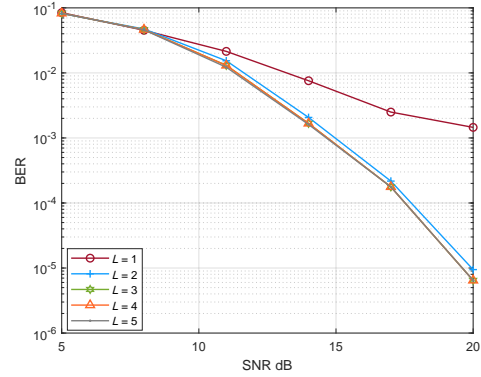


Fig. 6. BER vs. SNR for the belief consensus-based cooperative EP detection with different iterations.

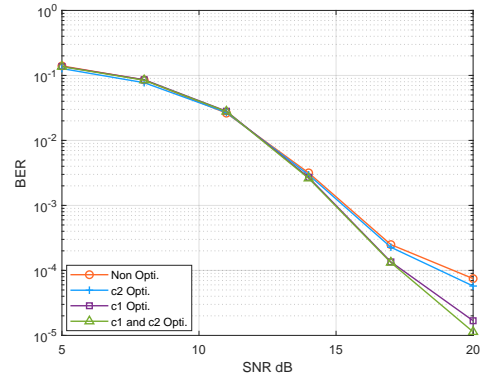
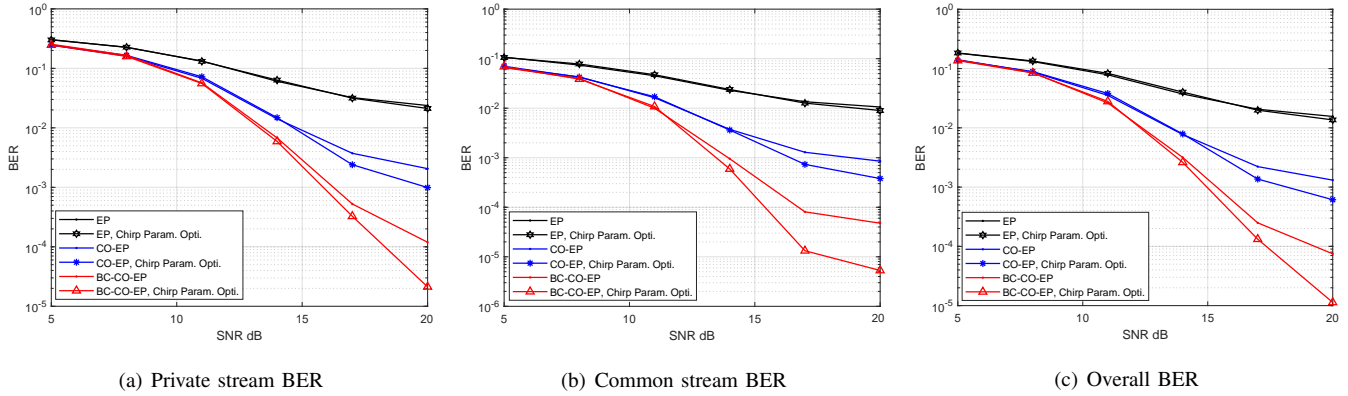
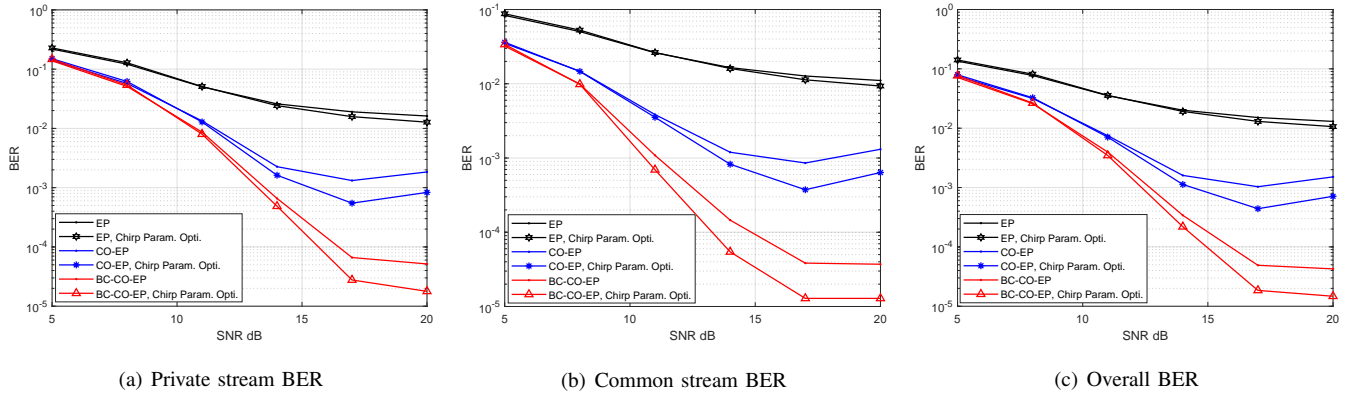


Fig. 7. BER vs. SNR for the proposed belief consensus-based cooperative scheme with different parameter optimizations.

scheme. NOMA-AFDM is used as the benchmark. The power allocation for the common stream in RSMA and for the far user in NOMA is set to 0.9, and the MMSE detection is adopted in both schemes. As shown in Fig. 5, the multi-antenna spatial diversity effectively suppresses the interference among different users; therefore, RSMA-AFDM outperforms NOMA-AFDM. Moreover, as N_t increases, the performance gain achieved by RSMA-AFDM becomes significantly larger than that of NOMA-AFDM. This indicates that RSMA-AFDM can fully exploit the spatial multiplexing gain, whereas NOMA-AFDM, which is originally designed for single-antenna systems, cannot effectively leverage this advantage.


 Fig. 8. BER vs. SNR for private stream, common stream, and overall system with $N_t = 4$ and $K = 2$.

 Fig. 9. BER vs. SNR for private stream, common stream, and overall system with $N_t = 8$ and $K = 2$.

In addition, the proposed chirp parameter optimization scheme further improves the performance of RSMA-AFDM.

Next, we focus on the cooperative RSMA-AFDM system. We first investigate the impact of the iteration number L on the proposed belief consensus EP-based distributed cooperative detector. Fig. 6 shows the simulated BER performance for different values of L . The results show that the algorithm converges rapidly as L increases: after only two iterations, the performance improves significantly and is already close to the optimum; when $L = 3$, the performance curve becomes almost flat, and further increasing L yields negligible additional gain. This rapid convergence characteristic indicates that the proposed belief consensus EP-based cooperative detection algorithm can effectively exploit cooperative information. Based on this observation, we set $L = 3$ in all subsequent simulations to achieve a balance between detection performance and computational complexity.

Here, we study the impact of the chirp-parameter choices on system performance. As shown in Fig. 7, the optimization of the parameter c_2 has a limited impact on detection performance. This is because c_2 does not change the position, spacing, or overlap of equivalent channel paths in the DAFT domain and therefore has minimal effect on the channel structure seen by the detector. In contrast, the parameter c_1 plays a crucial role: it directly affects the slope of the chirp signal and is key to ensuring that all propagation paths in the DAFT domain are separable. The proposed c_1 optimization scheme,

which assigns different c_1 values to different users, effectively reduces the overlap among their equivalent channels and yields considerable cooperative diversity gain. As optimizing both c_1 and c_2 improves performance, subsequent simulations use their simultaneous optimization.

Then, we evaluate the joint effect of chirp-parameter optimization and cooperative EP detection in the RSMA-AFDM system. The system is configured with $N_t = 4$ and $N_t = 8$ for $K = 2$. We examine the BER of the common stream, the private streams, and the overall system, as shown in Figs. 8 and 9. The results indicate that the proposed chirp parameter optimization scheme yields significant performance gain for cooperative detection, particularly for the common stream detection. By reshaping the DAFT domain equivalent channel, the proposed chirp parameter optimization method increases the achievable diversity gain for common-stream detection and thus yields a larger improvement in common-stream BER. In addition, both proposed cooperative EP detection schemes significantly outperform the non-cooperative EP detection, demonstrating the significant improvement in system reliability provided by the cooperative mechanism. Furthermore, the belief consensus-based cooperative detection scheme achieves a noticeably lower BER than the decision fusion-based scheme. This is because the belief consensus-based cooperative scheme more fully exploits the diversity gain, and more effectively mitigates the interference from the private stream components during the common stream

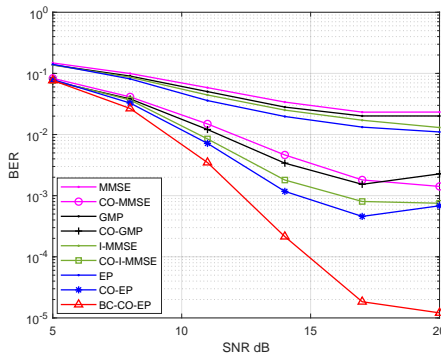


Fig. 10. BER vs. SNR for different detection schemes with $N_t = 8$, $K = 2$.

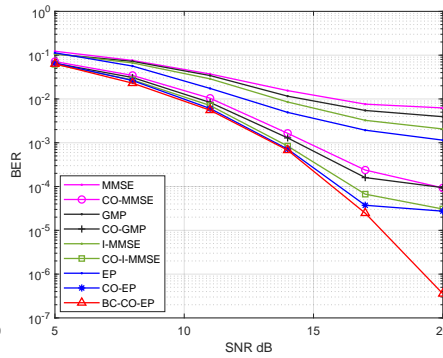


Fig. 11. BER vs. SNR for different detection schemes with $N_t = 8$, $K = 2$ and $p_c = 0.8$.

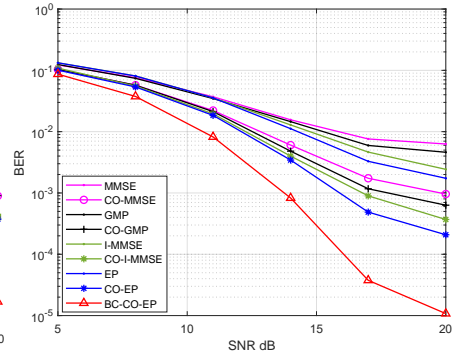


Fig. 12. BER vs. SNR for different detection schemes with 5 dB cooperative link performance loss.

detection process through multi-user cooperation.

Here, we compare the performance of the two proposed distributed cooperative detection schemes with that of other detection schemes. All algorithms employ the proposed chirp parameter optimization scheme. Additionally, benchmark algorithms with cooperative strategies are evaluated, all of which adopt the proposed decision fusion-based distributed cooperative detection mechanism. As shown in Fig. 10, all cooperative detection schemes achieve significant performance gain compared with non-cooperative schemes. Cooperative detection can effectively exploit the channel diversity among different users, thereby achieving higher diversity gain and resulting in notable SNR improvements. Leveraging the powerful detection capability of the EP algorithm, the proposed decision fusion-based EP scheme outperforms cooperative MMSE, cooperative GMP, and cooperative I-MMSE. Furthermore, the proposed belief consensus-based cooperative detection scheme exhibits clearly superior performance compared with other schemes. Through multiple rounds of distributed exchange and fusion of first- and second-order statistical information among cooperating users, this scheme forms more consistent decision. Moreover, at high SNR, the BER curves of different schemes saturate because the interference from the private-stream components limits the common-stream detection.

Fig. 11 presents the results for $p_c = 0.8$, where N_t is set to 8. Increasing the common-stream power improves the convergence performance because the interference from the private-stream components is reduced. However, the additional gain provided by cooperative detection becomes smaller, since less interference remains to be mitigated. This observation indirectly confirms the effectiveness of the proposed schemes in suppressing interference and enhancing system reliability.

In practical communication systems, cooperative links often experience certain performance degradation. To verify that the proposed cooperative detection methods remain effective under such conditions, we perform simulations with $N_t = 8$ and $p_c = 0.8$, while introducing a 5 dB loss on the cooperative link. As shown in Fig. 12, even with this degradation, the proposed belief consensus EP-based cooperative detection scheme still provides substantial gain over other schemes. This result demonstrates that the proposed belief consensus-based scheme exhibits strong robustness and can effectively enhance

system reliability under practical channel conditions.

VII. CONCLUSION

This paper proposes a cooperative RSMA-AFDM system and provides a performance analysis. We demonstrate that the system achieves maximum diversity gain when the overlap of the DAFT domain equivalent channel column spaces of different users is minimized. Based on this result, we design a chirp-parameter optimization scheme for AFDM to reduce this overlap. To further exploit the diversity gain, we develop a decision-fusion distributed cooperative detection scheme and a belief-consensus-based cooperative EP scheme. The latter mitigates the adverse impact of inaccurate prior variances by exploiting the symbol statistics exchanged during the EP iterations. Simulation results show that both proposed cooperative detection schemes converge rapidly and significantly improve detection performance. The results also verify that the proposed chirp optimization scheme effectively reduces inter-user interference and enhances cooperative diversity gain, with the slope of the AFDM chirp parameter. Overall, the results indicate that integrating cooperative RSMA with AFDM is a promising approach for future wireless systems operating over doubly selective channels.

REFERENCES

- [1] J. Chen, X. Wang, and L. Hanzo, "OTFS-MDMA: An elastic multi-domain resource utilization mechanism for high mobility scenarios," *IEEE J. Sel. Areas Commun.*, vol. 43, no. 4, pp. 1405–1420, Apr. 2025.
- [2] S. Li, W. Yuan, C. Liu, Z. Wei, J. Yuan, B. Bai, and D. W. K. Ng, "A novel ISAC transmission framework based on spatially-spread orthogonal time frequency space modulation," *IEEE J. Sel. Areas Commun.*, vol. 40, no. 6, pp. 1854–1872, Jun. 2022.
- [3] R. Hadani, S. Rakib, M. Tsatsanis, A. Monk, A. J. Goldsmith, A. F. Molisch, and R. Calderbank, "Orthogonal time frequency space modulation," in *Proc. IEEE Wireless Commun. Netw. Conf. (WCNC)*. San Francisco, CA, USA: IEEE, Mar. 2017, pp. 1–6.
- [4] S. Li, J. Yuan, W. Yuan, Z. Wei, B. Bai, and D. W. K. Ng, "Performance analysis of coded OTFS systems over high-mobility channels," *IEEE Trans. Wireless Commun.*, vol. 20, no. 9, pp. 6033–6048, Sep. 2021.
- [5] H. Qu, G. Liu, M. A. Imran, S. Wen, and L. Zhang, "Efficient channel equalization and symbol detection for MIMO OTFS systems," *IEEE Trans. Wireless Commun.*, vol. 21, no. 8, pp. 6672–6686, Aug. 2022.
- [6] S. Li, W. Yuan, Z. Wei, and J. Yuan, "Cross domain iterative detection for orthogonal time frequency space modulation," *IEEE Trans. Wireless Commun.*, vol. 21, no. 4, pp. 2227–2242, Apr. 2022.

- [7] P. Raviteja, K. T. Phan, and Y. Hong, "Embedded pilot-aided channel estimation for OTFS in delay-Doppler channels," *IEEE Trans. Veh. Technol.*, vol. 68, no. 5, pp. 4906–4917, May 2019.
- [8] Z. Wei, W. Yuan, S. Li, J. Yuan, G. Bharatula, R. Hadani, and L. Hanzo, "Orthogonal time-frequency space modulation: A promising next-generation waveform," *IEEE Wireless Commun.*, vol. 28, no. 4, pp. 136–144, Aug. 2021.
- [9] A. Bemani, N. Ksairi, and M. Kountouris, "Affine frequency division multiplexing for next generation wireless communications," *IEEE Trans. Wireless Commun.*, vol. 22, no. 11, pp. 8214–8229, Mar. 2023.
- [10] G. Liu, T. Mao, Z. Xiao, M. Wen, R. Liu, J. Zhao, E. Basar, Z. Wang, and S. Chen, "Pre-chirp-domain index modulation for full-diversity affine frequency division multiplexing toward 6G," *IEEE Transactions on Wireless Communications*, vol. 24, no. 9, pp. 7331–7345, Sep. 2025.
- [11] H. Yin, X. Wei, Y. Tang, and K. Yang, "Diagonally reconstructed channel estimation for MIMO-AFDM with inter-Doppler interference in doubly selective channels," *IEEE Trans. Wireless Commun.*, vol. 23, no. 10, pp. 14 066–14 079, Oct. 2024.
- [12] Y. Tao, M. Wen, Y. Ge, J. Li, E. Basar, and N. Al-Dhahir, "Affine frequency division multiplexing with index modulation: Full diversity condition, performance analysis, and low-complexity detection," *IEEE J. Sel. Areas Commun.*, vol. 43, no. 4, pp. 1041–1055, Apr. 2025.
- [13] Q. Li, J. Li, M. Wen, X. Dang, H. Arslan, and N. Al-Dhahir, "Affine frequency division multiplexing for 6G networks: Fundamentals, opportunities, and challenges," *IEEE Netw.*, 2025, early access, doi:10.1109/MNET.2025.3569668.
- [14] H. S. Rou, G. T. F. de Abreu, J. Choi, D. González G., M. Kountouris, Y. L. Guan, and O. Gonsa, "From orthogonal time-frequency space to affine frequency-division multiplexing: A comparative study of next-generation waveforms for integrated sensing and communications in doubly dispersive channels," *IEEE Signal Process. Mag.*, vol. 41, no. 5, pp. 71–86, Sep. 2024.
- [15] Q. Li, G. Liu, Y. Liu, H. Liu, F. Xu, and C. Liu, "Deep learning aided low complexity expectation propagation turbo detection for AFDM," *IEEE Trans. Commun.*, 2025, early access, doi:10.1109/TCOMM.2025.3635776.
- [16] V. Khammammetti and S. K. Mohammed, "OTFS-based multiple-access in high Doppler and delay spread wireless channels," *IEEE Wireless Commun. Lett.*, vol. 8, no. 2, pp. 528–531, Apr. 2019.
- [17] K. Deka, A. Thomas, and S. Sharma, "OTFS-SCMA: A code-domain NOMA approach for orthogonal time frequency space modulation," *IEEE Trans. Commun.*, vol. 69, no. 8, pp. 5043–5058, Aug. 2021.
- [18] H. Wen, W. Yuan, Z. Liu, and S. Li, "OTFS-SCMA: A downlink NOMA scheme for massive connectivity in high mobility channels," *IEEE Trans. Wireless Commun.*, vol. 22, no. 9, pp. 5770–5784, Sep. 2023.
- [19] K. Zheng, M. Wen, T. Mao, L. Xiao, and Z. Wang, "Channel estimation for AFDM with superimposed pilots," *IEEE Trans. Veh. Technol.*, vol. 74, no. 2, pp. 3389–3394, Feb. 2025.
- [20] Q. Luo, P. Xiao, Z. Liu, Z. Wan, N. Thomos, Z. Gao, and Z. He, "AFDM-SCMA: A promising waveform for massive connectivity over high mobility channels," *IEEE Trans. Wireless Commun.*, vol. 23, no. 10, pp. 14 421–14 436, Oct. 2024.
- [21] S. Li, Z. Wei, W. Yuan, J. Yuan, B. Bai, D. W. K. Ng, and L. Hanzo, "Faster-than-Nyquist asynchronous NOMA outperforms synchronous NOMA," *IEEE J. Sel. Areas Commun.*, vol. 40, no. 4, pp. 1128–1145, Apr. 2022.
- [22] A. Chatterjee, V. Rangamgari, S. Tiwari, and S. S. Das, "Nonorthogonal multiple access with orthogonal time-frequency space signal transmission," *IEEE Syst. J.*, vol. 15, no. 1, pp. 383–394, Mar. 2021.
- [23] Y. Xu, Z. Du, W. Yuan, S. Jia, and V. C. M. Leung, "Performance of OTFS-NOMA scheme for coordinated direct and relay transmission networks in high-mobility scenarios," *IEEE Wireless Commun. Lett.*, vol. 12, no. 12, pp. 2268–2272, Dec. 2023.
- [24] Y. Zhou, Z. Li, J. Shi, P. Xiao, and R. Tafazolli, "Resource allocation of OTFS-NOMA-based mmW communication for heterogeneous mobility users," *IEEE Trans. Commun.*, 2025, early access, doi:10.1109/TCOMM.2025.3610217.
- [25] B. Clerckx, Y. Mao, R. Schober, E. A. Jorswieck, D. J. Love, J. Yuan, L. Hanzo, G. Y. Li, E. G. Larsson, and G. Caire, "Is NOMA efficient in multi-antenna networks? a critical look at next generation multiple access techniques," *IEEE Open J. Commun. Soc.*, vol. 2, pp. 1310–1343, 2021.
- [26] H. Jafarkhani, H. Maleki, and M. Vaezi, "Modulation and coding for NOMA and RSMA," *Proc. IEEE*, vol. 112, no. 9, pp. 1179–1213, Sep. 2024.
- [27] Y. Mao, O. Dizdar, B. Clerckx, R. Schober, P. Popovski, and H. V. Poor, "Rate-splitting multiple access: Fundamentals, survey, and future research trends," *IEEE Commun. Surv. Tutorials*, vol. 24, no. 4, pp. 2073–2126, 4th Quart. 2022.
- [28] X. Lyu, S. Aditya, J. Kim, and B. Clerckx, "Rate-splitting multiple access: The first prototype and experimental validation of its superiority over SDMA and NOMA," *IEEE Trans. Wireless Commun.*, vol. 23, no. 8, pp. 9986–10 000, Aug. 2024.
- [29] Y. Wang, V. W. S. Wong, and J. Wang, "Flexible rate-splitting multiple access with finite blocklength," *IEEE J. Sel. Areas Commun.*, vol. 41, no. 5, pp. 1398–1412, May 2023.
- [30] Y. Mao, B. Clerckx, and V. O. Li, "Rate-splitting multiple access for downlink communication systems: Bridging, generalizing, and outperforming SDMA and NOMA," *EURASIP J. Wirel. Commun. Netw.*, vol. 2018, no. 1, p. 133, 2018.
- [31] B. Clerckx, H. Joudeh, C. Hao, M. Dai, and B. Rassouli, "Rate splitting for MIMO wireless networks: A promising PHY-layer strategy for LTE evolution," *IEEE Commun. Mag.*, vol. 54, no. 5, pp. 98–105, May 2016.
- [32] Y. Zhang, W. Xia, H. Zhao, Y. Mao, J. Zhang, and G. Zheng, "Enhancing uplink performance for Cell-free massive MIMO with low-resolution ADCs by RSMA," *IEEE J. Sel. Areas Commun.*, vol. 43, no. 3, pp. 720–735, Mar. 2025.
- [33] T. P. Truong, T. M. T. Nguyen, T. V. Nguyen, N.-N. Dao, and S. Cho, "Energy efficiency in RSMA-enhanced active RIS-aided quantized downlink systems," *IEEE J. Sel. Areas Commun.*, vol. 43, no. 3, pp. 834–850, Mar. 2025.
- [34] Z. Li, S. Han, M. Peng, C. Li, and W. Meng, "Dynamic multiple access based on RSMA and spectrum sharing for integrated satellite-terrestrial networks," *IEEE Trans. Wireless Commun.*, vol. 23, no. 6, pp. 5393–5408, Jun. 2024.
- [35] J. Huang, Y. Yang, J. Lee, D. He, and Y. Li, "Deep reinforcement learning-based resource allocation for RSMA in leo satellite-terrestrial networks," *IEEE Trans. Commun.*, vol. 72, no. 3, pp. 1341–1354, Mar. 2024.
- [36] B. Clerckx, Y. Mao, E. A. Jorswieck, J. Yuan, D. J. Love, E. Erkip, and D. Niyato, "A primer on rate-splitting multiple access: Tutorial, myths, and frequently asked questions," *IEEE J. Sel. Areas Commun.*, vol. 41, no. 5, pp. 1265–1308, May 2023.
- [37] Z. Liu, W. Chen, Q. Wu, Z. Li, Q. Wu, N. Cheng, and J. Li, "Beamforming design and multi-user scheduling in transmissive RIS enabled distributed cooperative ISAC networks with RSMA," *IEEE Trans. Commun.*, 2025, early access, doi:10.1109/TCOMM.2025.3594771.
- [38] P. Gao, L. Lian, and J. Yu, "Cooperative ISAC with direct localization and rate-splitting multiple access communication: A pareto optimization framework," *IEEE J. Sel. Areas Commun.*, vol. 41, no. 5, pp. 1496–1515, May 2023.
- [39] Z. Xu, S. Xu, H. Ding, and B. Ai, "A rate-splitting multiple access enabled cooperative ISAC tracking system for complex V2I scenarios," *IEEE Trans. Veh. Technol.*, 2025, early access, doi:10.1109/TVT.2025.3607006.
- [40] J. Yang, S. Gao, Y. Lu, and G. Tu, "CoMP-assisted cooperative RSMA for indoor aggregated VLC/RF cellular systems," *IEEE Internet Things J.*, vol. 12, no. 18, pp. 38 631–38 644, Sep. 2025.
- [41] A. Salem, C. Masouros, and B. Clerckx, "Secure rate splitting multiple access: How much of the split signal to reveal?" *IEEE Trans. Wireless Commun.*, vol. 22, no. 6, pp. 4173–4187, Jun. 2023.
- [42] Q. Li, G. Liu, Y. Zhao, C. Liu, and F. Xu, "Deep learning-based downlink OTFS-SCMA," *IEEE Wireless Commun. Lett.*, vol. 13, no. 12, pp. 3434–3438, Dec. 2024.
- [43] S. McWade, A. Farhang, and M. F. Flanagan, "Low-complexity reliability-based equalization and detection for OTFS-NOMA," *IEEE Trans. Commun.*, vol. 71, no. 11, pp. 6779–6792, Nov. 2023.
- [44] K. S. Ali, A. Al-Dweik, E. Hossain, and M. Chafii, "Physical layer security of partial-NOMA and NOMA in poisson networks," *IEEE Trans. Wireless Commun.*, vol. 23, no. 6, pp. 6562–6579, Jun. 2024.
- [45] W. Yuan, S. Li, Z. Wei, Y. Li, and P. Fan, "On hybrid detection of wireless communications over interference channels: A generalized framework," *IEEE J. Sel. Areas Commun.*, vol. 43, no. 4, pp. 1214–1229, Apr. 2025.
- [46] A. Kosasih, V. Onasis, V. Miloslavskaya, W. Hardjawana, V. Andrian, and B. Vucetic, "Graph neural network aided MU-MIMO detectors," *IEEE J. Sel. Areas Commun.*, vol. 40, no. 9, pp. 2540–2555, Sep. 2022.
- [47] L. Wu, S. Luo, D. Song, F. Yang, R. Lin, and S. Xie, "AFDM signal detection based on message passing scheme," *Digit. Signal Process.*, vol. 153, p. 104633, Jun. 2024.
- [48] Z. Li, C. Zhang, G. Song, X. Fang, X. Sha, and D. T. M. Slock, "Chirp parameter selection for affine frequency division multiplexing with MMSE equalization," *IEEE Trans. Commun.*, vol. 73, no. 7, pp. 5079–5093, Jul. 2025.